Theoretical investigation on the fluorescent sensing mechanism for recognizing formaldehyde: TDDFT calculation and excited-state nonadiabatic dynamics

Yunfan Yang(杨云帆)[1,3,†], Lujia Yang(杨璐佳)[1], Fengcai Ma(马凤才)[2], Yongqing Li(李永庆)[2,‡], and Yue Qiu(邱岳)[4]

[1] *Key Laboratory for Microstructural Material Physics of Hebei Province, School of Science, Yanshan University, Qinhuangdao* 066004, *China*
[2] *Department of Physics, Liaoning University, Shenyang* 110036, *China*
[3] *State Key Laboratory of Molecular Reaction Dynamics, Dalian Institute of Chemical Physics, Chinese Academy of Sciences, Dalian* 116023, *China*
[4] *Grimwade Centre for Cultural Materials Conservation, School of Historical and Philosophical Studies, Faculty of Arts University of Melbourne, Parkville, VIC* 3052, *Australia*

(Received 2 June 2022; revised manuscript received 29 June 2022; accepted manuscript online 13 July 2022)

Inspired by the activity-based sensing method, the hydrazine-modified naphthalene derivative (Naph1) was synthesized and used as a fluorescent probe to detect formaldehyde (FA) in living cells. Through the condensation reaction between the probe Naph1 and analyte FA, researchers observed a ∼ 14 folds enhancement of fluorescent signal around 510 nm in an experiment, realizing the high selectivity and sensitivity detection of FA. However, a theoretical understanding of the sensing mechanism was not provided in the experimental work. Given this, the light-up fluorescent detecting mechanism was in-depth unveiled by performing the time-dependent density functional theory (TDDFT) and the complete active space self-consistent field (CASSCF) theoretical calculations on excited-state intramolecular proton transfer (ESIPT) and non-adiabatic excited-state dynamics simulation. The deactivation channel of S_1/T_2 intersystem crossing (ISC) was turned off to successfully recognize FA. Insight into the ESIPT-based fluorescent detecting mechanism indicated that ESIPT was essential to light-up fluorescent probes. This work would provide a new viewpoint to develop ESIPT-based fluorescent probes for detecting reactive carbon species *in vivo* or *vitio*.

Keywords: proton transfer, twisting intramolecular charge transfer, intersystem crossing, fluorescent probe

PACS: 78.47.da, 33.15.Hp, 87.15.ht, 33.20.–t **DOI:** 10.1088/1674-1056/ac80af

1. Introduction

Formaldehyde (FA), one of the most critical reactive carbon species (RCS), has attracted extensive attention in chemical industries and laboratories because of its extreme toxicity and accessibility.[1] As early as the 1980s, a few advanced works of literature at that time have reported that FA was widely applied in some chemical industries as a synthetic reactant for plastics, cosmetics, wood processing, drugs, and food,[2–5] especially acting as a preservative existed in daily food.[6] Hence, environmental FA mainly originates from the above chemical activities. We have to admit that favorable FA concentrations play crucial roles in physiological activity.[7,8] In comparison, aberrant environment exposure to FA is detrimental to biomolecules and cell function, which at worst causes DNA damage, Alzheimer's, cancer, even death.[9–11] FA was defined by the International Agency for Research on Cancer as human carcinogen group I in 2004.[12] The roles of FA have not been well-defined so far, presumably because of a lack of sensitive and selective molecular tools for investigating FA in environmental and endogenous systems, which motivates to develop new methods for monitoring FA to help decipher its native function.[13]

Most contemporary researchers have developed many measurements to detect reactive one-carbon species such as electro-fluorescent biosensors, piezoelectric sensors, fluorescent probes, Raman spectroscopy, transmission electromicroscopy, etc.[14] For small RCS like FA, fluorescent probes are based on the reactivities of analytes instead of specific lock-and-key binding detection. The distinct changes of fluorescent signals are presented by chemical reactions between the probes and target, achieving the selective detecting for FA. The high sensitivity, selectivity, and low limit of detection of fluorescent probes successfully enable biological analysis of FA in living systems.[13] Recently, Liu's group reviewed and discussed the valuable developments in the fluorescent probes for detecting FA.[15] Two main detecting mechanisms are introduced. (i) The aza-cope rearrangement reaction of the homoallylamino group and FA produces fluorescent-mutated aldehyde or phenolic species. (ii) The condensation reaction between amino/hydrazine group and FA produces formimine-/methylene-hydrazine, inducing fluorescent signal changes. The aza-cope rearrangement is excellent selectivity and high sensitivity, but its synthetic procedure and the response to FA are complicated and slow respectively.[15] Flu-

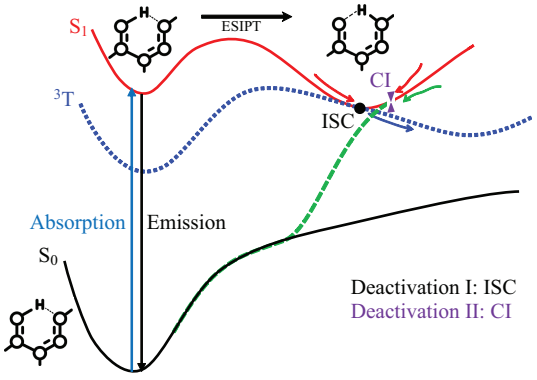
†Corresponding author. E-mail: yangyunfan2626@163.com
‡Corresponding author. E-mail: yqli@lnu.edu.cn

© 2023 Chinese Physical Society and IOP Publishing Ltd

orescent probes based on condensation reaction have a fast response to FA, which makes up for the deficiency of aza-cope rearrangement.[16] Moreover, hydrazine compounds have low cytotoxicity that could be successfully applied to detect FA in living cells, which is something that fluorescent probe formimine-based cannot compare.

Fundamental photophysical processes such as photoinduced electron transfer, intramolecular charge transfer, Förster/Dexter energy transfer, and intramolecular motion restriction are the above fluorescent probe detecting mechanisms.[17] A well-known photochemical reaction, excited-state intramolecular proton transfer (ESIPT), is spontaneous and takes on a faster time scale than fluorescent radiation. So, the typical dual-fluorescent phenomena of ESIPT chromophore are exhibited. Moreover, ESIPT emission usually has an enormous Stoke's shift that the self-absorption or the inner filter effect of the chromophore is hindered, which is favorable to enhance the fluorescent signal for detecting analytes.[18–20] More importantly, plenty of experiments and theoretical researches have argued that the molecular photophysical processes can be fine-tuned by changing substituent and solvent effects on ESIPT reactions.[21–30] For example, the design and synthesis of fluorescent probes via modulating the substituent effects on ESIPT was reported.[31–34]

The ESIPT reaction is often accompanied by strong geometric structure twist or intramolecular charge transfer, resulting in fluorescence quenching. Alternatively, the ESIPT processes could turn on the deactivation channels of intersystem crossing (ISC) or conical intersection (CI), as shown in Scheme 1. The ISC involved in the spin reversal of electron occurs between singlet and triplet excited states, and the CI occurs in crossings between two adiabatic potential surfaces (singlet excited and ground states). Which deactivation channel is "turn-on" or "turn-off" is an important investigation to reveal the detecting mechanisms of light-up fluorescent probes.



Scheme 1. Two deactivation channels of ESIPT processes. The ISC represents the intersystem crossing point of the first singlet excited (S_1), and triplet (^3T) states; the green dash line represents ground (S_0) state potential surface as allowing non-adiabatic electronic transitions to occur.

Jiang's group designed and synthesized a light-up ESIPT-based fluorescent probe naphthalene derivative (Naph1) in 2019. They proposed that the hydrazone product generated by the chemical reaction between NaPh1 and analyte FA enhances the ICT degree, activating the fluorescent signal for detecting FA.[15] However, the detection mechanism of light-up fluorescent probe Naph1 will be relative to the deactivation channel turn on or off. In our research work, the detection mechanism of light-up fluorescent probe Naph1 for FA is to be illustrated in-depth.

2. Methods

In our research, we used the universal solvation model SMD[35] to perform all self-consistent reaction field (SCRF) calculations, in which the static and dynamic dielectric constants (eps and epsinf) were specified as 75.20237 and 1.81196, respectively, to simulate the PBS buffer. The geometries of Naph1 and product for detecting FA were fully optimized with B3LYP/6-311G (d, p) level of theory, and then their infrared vibrational frequencies were calculated by the same theoretical method as geometric optimization. Free from imaginary frequency indicates that they are locally the most stable structures. Because B3LYP functional usually overrates the delocalization of electron[36] and underrates the transition energies,[37] the long-range correction functional CAM-B3LYP and 6-311G (d, p) basis set were used to evaluate the change of electron structures and transition energies. The excited-state calculation and dynamics simulation were performed based on the time-dependent density functional theory (TDDFT) method. TD-B3LYP/6-311G (d, p) was used to build potential energy surfaces and calculate the excited-state electronic energies. Dispersion corrections (version D3) were also included in these calculations.[38,39] To economize the calculation time, TD-B3LYP/6-31G (d) was carried out the excited-state non-adiabatic dynamics simulation of three lowest singlet excited states by Newton-X program.[40] To perform CASSCF calculation in gas phase, five π bonds and five π antibonding orbitals acted as the active spaces and electrons were chosen. The geometries and energies of S_1/S_0 minimum energy conical intersection (MECI) were optimized and calculated via SA-CASSCF (10o, 10e)/6-31G (d, p) theoretical level. Besides, the minimum energy crossing point (MECP) between the singlet and triplet states was sought out by sob-MECP program,[41] which was a modified version of MECP program developed by Harvey *et al.*[42] We used the DFT method to optimize and calulacte the molecular configurations and corresponding electronic energies in different electronic states. The effective gradients f and g of electronic energies were defined as

$$f = (E_1 - E_2)\left[\left(\frac{\partial E_1}{\partial q}\right) - \left(\frac{\partial E_2}{\partial q}\right)\right] = (E_1 - E_2)x_1, \quad (1)$$

$$g = \left(\frac{\partial E_1}{q}\right) - \frac{x_1}{|x_1|}\left[\left(\frac{\partial E_1}{\partial q}\right)\cdot\frac{x_1}{|x_1|}\right], \quad (2)$$

where E_1 and E_2 respectively were the single point energies of two different electronic states, and the electronic energies E_n and relative energy gradients $\partial E_n/\partial q$ for nuclear coordinates q were combined to obtain the effective gradients f and g. x_1 was energy gradient difference for two electronic states. The orthogonal vectors f and g went to zero at the MECP, in which the vector f acting as energy difference of two electronic states was perpendicular to the crossing hyperline on the two surfaces, and the vector g was parallel to that. However, the spin–orbit coupling effect was failed to be considered when we used DFT methods, and the electronic coupling matrix elements H_{12} and H_{21} became zero in two 2×2 Hessian matrices H_1 and H_2, therefore the obtained MECP was not a stable structure in $3N-6$ dimensions. In view of this, the energy of MECP would be corrected via second-order Taylor expansion for two electronic states

$$\begin{aligned} E &= E_{\mathrm{MECP}} + \frac{1}{2}\Delta q^{\mathrm{T}}\left[\left|\frac{\partial E_2}{\partial q}\right| H_2/|x_1| - \left|\frac{\partial E_2}{\partial q}\right| H_1/|x_1|\right]_{\Delta q} \\ &= E_{\mathrm{MECP}} + \frac{1}{2}\Delta q^{\mathrm{T}} H_{\mathrm{eff}} \Delta q, \end{aligned} \tag{3}$$

where Δq was the displacement along crossing hyperline, perpendicular to x_1. H_{eff} was diagonalization of the effective Hessian, which generated a set of $3N-7$ force constants along the crossing hyperline on two surfaces, so as to confirm the obtained MECP was a real minimum.[43]

The whole quantum chemistry theoretical computations were conducted with the Gaussian16 program.[44]

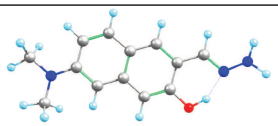
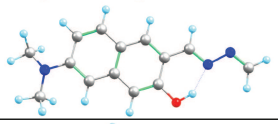
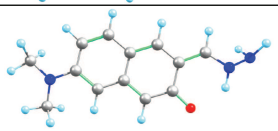
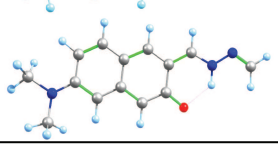
3. Results and discussion

3.1. Excitation transition calculation and fluorescent detection process

Before investigating the fluorescent sensing mechanism, the rationality of the chosen theoretical methods must be firstly validated by accurately reproducing the observed phenomena. Experimentally, the two distinctly different absorption wavelengths were observed during the detection of FA where the shorter peak about 330 nm was assigned to the absorption value of probe Naph1, and the more extended peak about 360 nm was attributed to that of hydrazone product.[15]

Based on the TDDFT method, the vertical excitation energies of localized, stable structures were calculated with TD-CAM-B3LYP-D3/6-311G (d, p) as shown in Table 1, which is well-matched with UV-vis absorption spectra values in the experiment (Fig. 1(a)). It indicates the correctness of geometric structure optimization and ensures the credibility of the following research on fluorescence detection mechanism. Notice that the absorption value of the product exhibits a red-shift of about 40 nm compared with that of Naph1, which may be because the condensation reaction between probe and analyte impacts electronic donor-acceptor properties of naphthalene skeleton, reflecting in molecular absorption energies.[13] Therefore, the hydrazine moiety of Naph1 acting as a potential reaction switch can be applied to recognize FA.

Table 1. The TDDFT-simulated transition energies between S_1 and S_0 states and corresponding composition indexes. The composition indexes larger than 75% indicate the main contribution to the transition from HOMO to LUMO. The theoretical level is TD-CAM-B3LYP-D3/6-311G (d, p)

Transition	Species	Configurations	Transitions energies (nm)	Composition indexes
Excitation	Naph1		$S_0\rightarrow S_1$ (325)	HOMO→LUMO (84%)
	Product		$S_0\rightarrow S_1$ (345)	HOMO→LUMO (91%)
De-excitation	Isomer of Naph1		$S_1\rightarrow S_0$ (−)	HOMO→LUMO (95%)
	Keto of product		$S_1\rightarrow S_0$ (552)	HOMO→LUMO (93%)

The activity-based sensing mechanism for detecting reactive carbon species FA exploited the reactive electrophiles of aldehydes instead of the lock-and-key detection.[45] The main reason Naph1 recognizes FA is that the active carbon atom of FA and the hydrazine N atom of Naph1 undergo dehydration condensation reaction. The reactive pathway and relevant reaction possibility cannot be given a quantitative description in the experiment. In our research, the transition state (TS) structures of condensation reaction were searched by Berny algorithm[46] to establish the reactive energy path-

way, in which the single point energies of reactants, TS and products have been corrected by Gibbs free energy, as shown in Fig. 2. This reaction involves three TS and two intermediate (IM) structures. Note that the free energy of TS2 lower than the IM1 is due to the overcorrection of Gibbs free energy.[47,48] The validity of TS structures is confirmed by calculating the intrinsic reaction coordinates (IRCs) in Fig. S1. Notice that the product's energy for detecting FA is lower than that of Naph1, which indicates that this reaction is thermodynamically feasible. In addition, the final by-product water in this reaction confirms that Naph1 has potential application for sensing biological FA because of its low cytotoxicity, high sensitivity, and superior selectivity to FA, showing that it is safely used to detect and identify FA in living cells.[15]

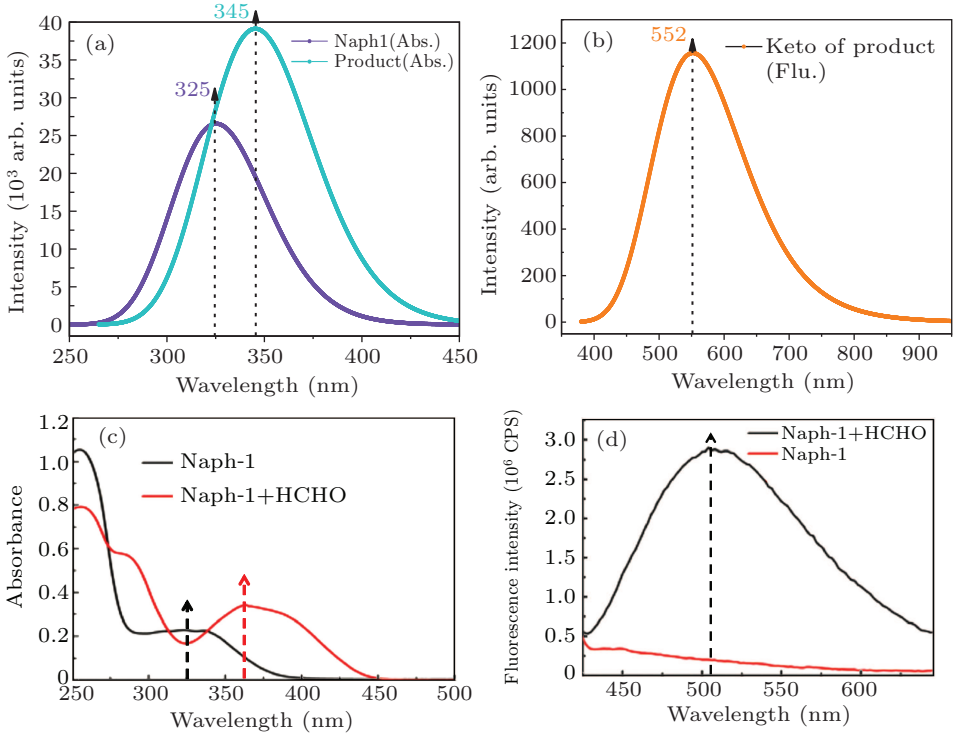


Fig. 1. The TDDFT-simulated vertical absorption spectra of Naph1 and product for detecting FA (a). The simulated emission spectra of keto of product (b). The observed absorption spectra of Naph1 and Naph1+HCHO (product) (c). The emission spectra of Naph1+HCHO (keto of product) (d) in the experiment. The graphs (c) and (d) are seen in Ref. [15].

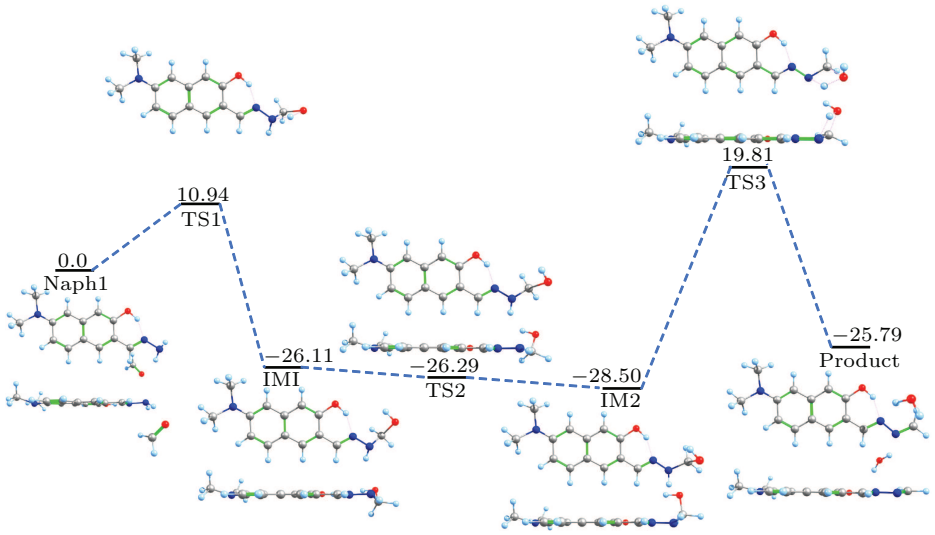


Fig. 2. The pathway of Gibbs free energy (kcal/mol) for the dehydration condensation between Naph1 and FA based on B3LYP-D3/6-311G (d, p) theoretical level. The top and side views of locally stable structures (Naph1 and product), transition state structures (TS), and intermediate structures (IM) are separately presented. (Unit is kcal/mol).

3.2. Excited state calculation and dynamics simulation

A fluorescent probe that relies on the reactivity of itself and analyte usually exhibits an intense fluorescent change, which is the most commonly sensing technique for efficient detection of small molecules. In Jiang group's research work, a nonemissive Naph1 probe that responded to FA showed a ∼

14 folds enhancement of fluorescent signal around 510 nm.[15] The calculated vertical emission energy of keto of product is presented in Table 1, in which the emissive values of 552 nm are consistent with that observed in the experiment (Fig. 1(b)), further demonstrating the reliability of theoretical calculation. The sensing mechanism was experimentally proposed that the amino group converts into the methylene group with a stronger electron-withdrawing capacity in the process of detecting FA, the fluorescence is turned on due to synergetic ICT and ESIPT effects. We agreed with the authors' viewpoint that ESIPT plays a crucial role in the sensing mechanism. However, a deeper understanding of the ESIPT-based fluorescent quenching mechanism is highly required. In Fig. 3, we built the potential energy surface as a function of O–H bond length and CNNH dihedral angle between naphthalene and amino group. The proton-transfer potential energy curves in S_0 and S_1 states are plotted (Fig. S2), and IRC graphs of reactive TS structures are exhibited (Fig. S3).

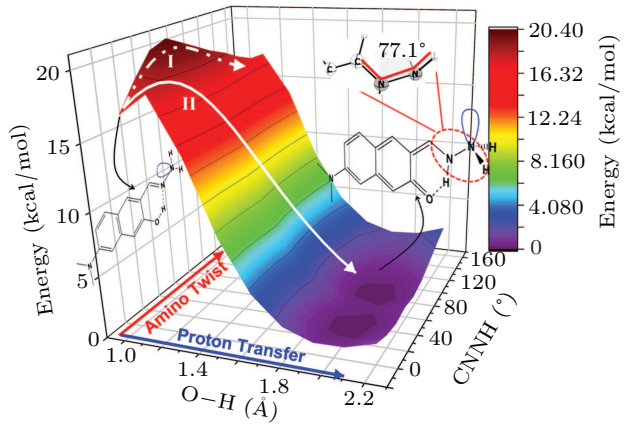


Fig. 3. Potential energy surface of Naph1 in S_1 state. The pathway I is the variations of Gibbs free energies as a function of torsion of CNNH dihedral angle; the pathway II is the variations of Gibbs free energies as a function of O–H bond length and CNNH dihedral angle.

The calculated activation energy barriers of ESIPT and its reversed process are 0.51 kcal/mol and 11.98 kcal/mol, respectively. Note that the energy of the isomer of Naph1 is 11.47 kcal/mol lower than Naph1, which shows that the isomer of Naph1 is the globally most stable structure. It follows that the ESIPT of pathway II occurs spontaneously, since the redistribution of electron density influences the proton donor-acceptor acidity and alkalinity upon the photoinduced process, which reinforces hydrogen bonding interaction to provide the essential driving force for ESIPT.[49–51] In addition, the dihedral angle of amino group and naphthalene of isomer of Naph1 is 77.1°, demonstrating that ESIPT accompanies this distortion of amino group. In stark contrast, the pathway I is the artificial distortion of CNNH dihedral angle without ESIPT, in which the distortion cannot occur. Some pieces of literature have reported that the substituent groups that are coplanar with fluorophore scaffolds are relaxed to out-plane form by ESIPT process, emerging the twisting intramolecular charge transfer (TICT) state.[52–56] Herein, the TICT state derived from ESIPT may be the key to turn on deactivation channels such as ISC or IC. Therefore, the relationship between ESIPT and TICT is vital to reveal the sensing mechanism for FA.

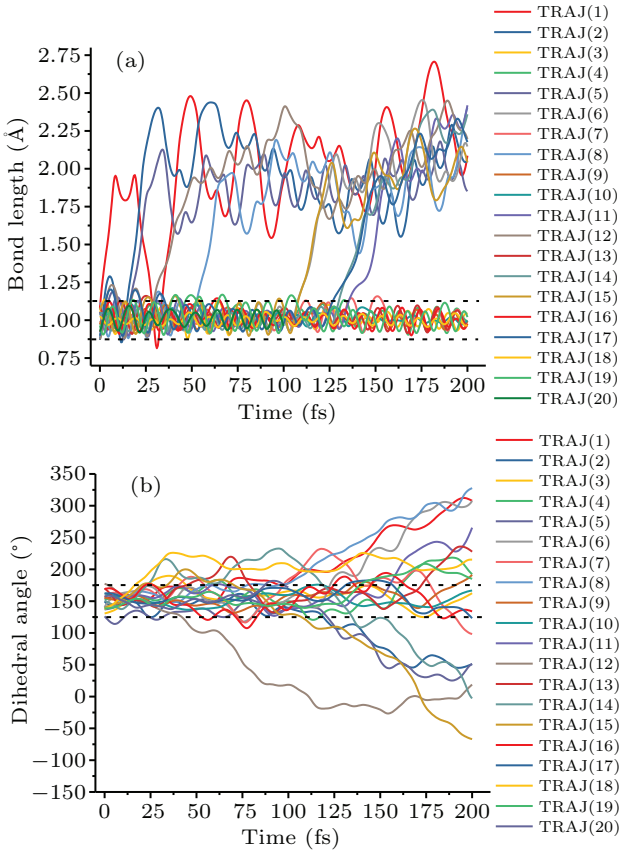


Fig. 4. Time evolution of excited-state dynamics for selected bond length (O–H) (a) and dihedral angle (CNNH) (b) along 20 trajectories based on the optimal Naph1 enolic form. The theoretical level is TD-B3LYP/6-31G (d).

To better shine some light on the relationship between ESIPT and TICT, the excited-state dynamics have been carried out by the TD-B3LYP/6-31G (d) level of theory. The small size basis set was used for saving computational resources. Total time evolution was set as 200 fs, the step size was fixed as 0.5 fs, and 20 trajectories from dynamics calculation started in S_1 state were generated based on non-adiabatic dynamic program Newton-X.[40] The time evolution of bond length (O–H) and dihedral angle (CNNH) were separately simulated as presented in Fig. 4, and it is found that ten of twenty trajectories exhibit the increase of O–H from initial about 1 Å (Fig. 4(a)). It is demonstrated that the ESIPT is a large possible to occur (50%). Note that the time scales of ESIPT reactions are less than 150 fs, indicating that the ESIPT reaction is a subpicosecond ultrafast process. Moreover, it is found from the time evolution of the dihedral angle (Fig. 4(b)) that the ten trajectories of ESIPT exhibit the distinct changes of the dihedral angle compared with the original $\sim 150°$, indicating the

synergetic relation of TICT and ESIPT. It concludes from reactive pathways and excited-state dynamics that the ESIPT induces the spontaneous rotation of the amino group of Naph1 to form a TICT, which could be the reason that turns on the deactivation channel. To give the molecule-level explanation on the fluorescent sensing mechanism, we described the frontier molecular orbitals of the isomer of Naph1 and keto of product for detecting FA.

3.3. Electronic effect analysis

Based on quantum chemistry calculation, the highest occupied and lowest unoccupied orbitals (HOMO and LUMO) are dominantly involved in the electron transition processes from S_1 to S_0 states, whose component indexes are larger than 75% (Table 1). The isosurfaces of HOMO and LUMO were drawn by Chemcraft program[57], as shown in Fig. 5. It should be noted that the electron transitions between HOMO and LUMO present the typical $\pi\pi^*$ character. According to the valance bond theory, each of the six-member rings of Naph1 attributes to Kekulé structures,[58] consisting of three C–C single bonds and three C=C double bonds. The electron density of the Kekulé structure is delocalized, and the Naph1 structure is favorable to be obtained.

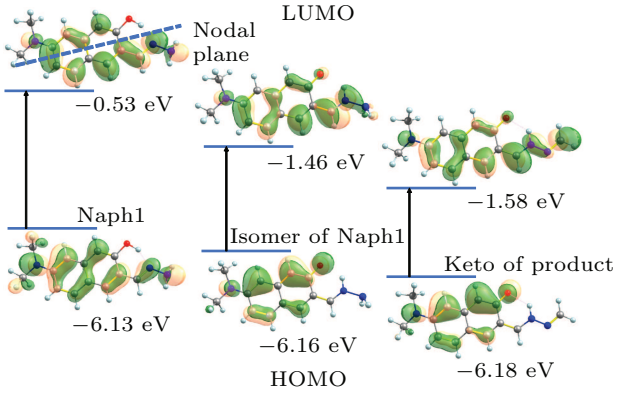


Fig. 5. Frontier molecular orbitals of typical and isomer forms of Naph1 and product for detecting FA. The blue dash line represents the nodal plane. The level of theory is TD-CAM-B3LYP/6-311G (d, p).

Interestingly, each of the six-member rings for an isomer of Naph1 has four C–C single bonds and two C=C double bonds after ESIPT occurs. The more localized electron population of isomer of Naph1 enhances the ICT degree, and the same conclusion is also acquired via the isosurfaces of frontier molecular orbitals (FMOs). In addition to ICT strengthening induced by ESIPT, the ESIPT reaction is favorable because the Kekulé structure tends to Schiff base in the S_1 state as the nodal model proposed by Nagaoka *et al.*[59,60] Compared with isomer of Naph1, the TICT is suppressed for keto of product due to loss of the amino group, which may restore the chromophoric function of the sensor. The analysis of FMOs provide a more profound insight into fluorescent sensing mechanisms, that is, turning off the deactivation channel is key to response to FA. Deactivation channel includes ISC and CI, the excited-state calculations on potential energy curves and dynamics simulation are essential to distinguish which nonradiative decay process contributes to the light-up fluorescent detecting for FA.

3.4. Illumination of fluorescent sensing mechanism

The energy pathways of singlet and triplet states and the dynamic trajectories of energies for S_0, S_1, and S_2 states are presented in Fig. 6. The time evolution of energy with ESIPT (Fig. 6(a)) and without ESIPT (Fig. 6(b)) originated from 20 trajectories are randomly selected, in which the energy differences of the lowest singlet states (S_0 and S_1) are higher than 0.20 eV, indicating that ESIPT process does not open CI deactivation channel. Based on the multi-configurational self-consistent field (MCSCF) theory, the state-averaged complete active space self-consistent field (SA-CASSCF) method and 6-31G (d, p) basis set were applied for searching the S_0/S_1 minimum energy conical intersection (MECI), in which the active spaces and electrons are 10 active orbitals and 10 active electrons. It follows that the MECI is nonexistent during the ESIPT process. It exists in the form of a broken intramolecular hydrogen bond, in which the whole hydrazine group is nearly perpendicular to the naphthalene skeleton, as shown in Fig. 7. In order to explore whether the reaction process that breaks intramolecular hydrogen bond takes place, the changes of electronic energies as function of the dihedral angle δ(CCCH) of probe molecule are performed as presented in Fig. 8. The established potential energy curves indicate that the MECI form is thermodynamically unstable because of the high energy barrier of 6.67 kcal/mol and the negligible reversed energy barrier of 0.60 kcal/mol. Therefore, the nonemissive Naph1 could be attributed to the ISC transition.

The ESIPT energy pathways of S_0, the six lowest singlet excited (S_1, S_2, S_3) and triplet (T_1, T_2, T_3) states, were built for Naph1 (Fig. 6(c)) and product (Fig. 6(d)). It is obvious from Fig. 6(c) that the S_1/T_2 ISC located at isomer of Naph1, which is also confirmed by searching the S_1/T_2 minimum energy crossing point (MECP) based on sobMECP program,[41] the energies, and coordinates of MECP between S_1 and T_2 states are shown in Tables S1 and S2. Note that the S_1/T_2 ISC deactivation channel is turned off along with the ESIPT reaction of the keto of product, as shown in Fig. 6(d). It concludes that the light-up Naph1 probe generates the hydrazone compound through a condensation reaction with FA to turn off the deactiavation channel, generating the strong fluorescent signal to realize the efficient detection for FA.

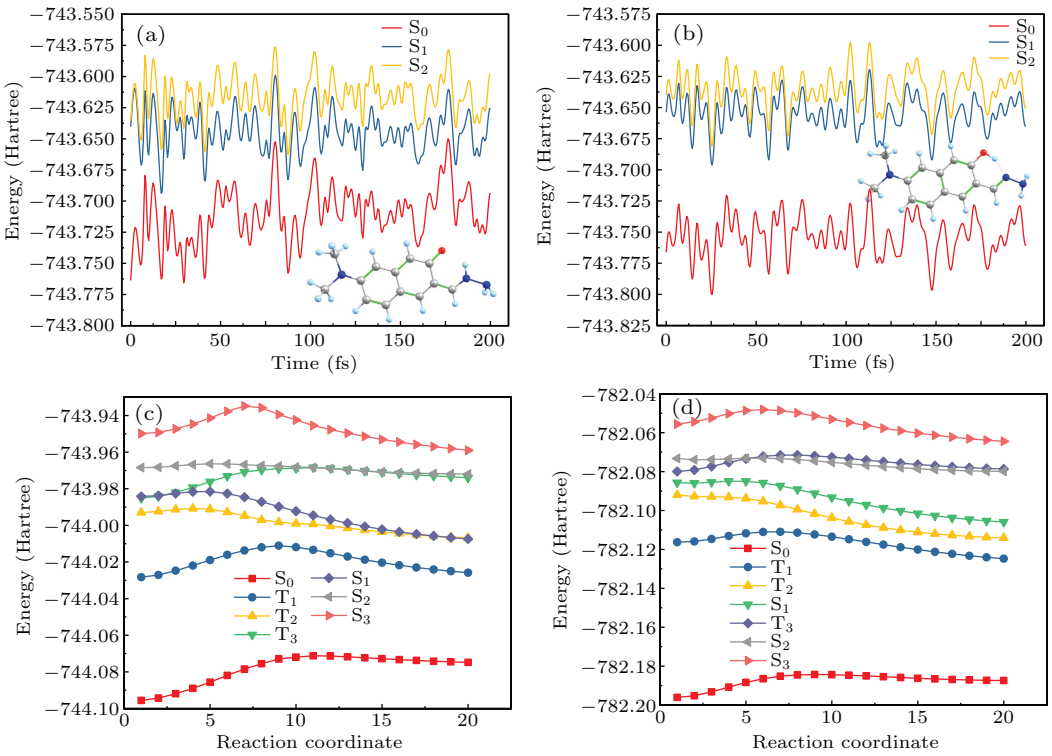


Fig. 6. Time evolution of electron energies of ESIPT occurring (a) and not occurring (b) in S_0, S_1, S_2 states. The ESIPT energy pathways of S_0, six lowest singlet excited (S_1, S_2, S_3) and triplet (T_1, T_2, T_3) states for Naph1 (c) and product (d).

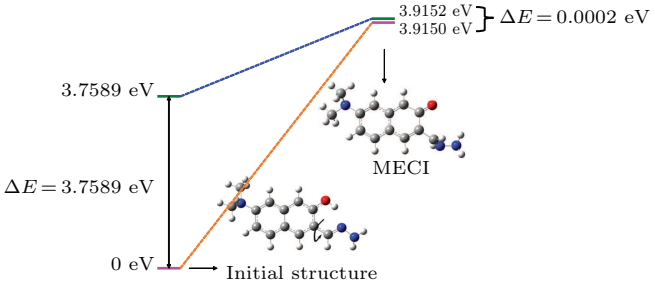


Fig. 7. Schematic diagram of the diabatic potential curves of the ground state (pink line) and excited state (dark green line). The optimized initial structure and MECI via CASSCF/6-31G (d, p) theoretical level in gas phase. Based on the state-average CASSCF method, the energy difference between different electronic states is 0.0002 eV, less than 0.2 eV.

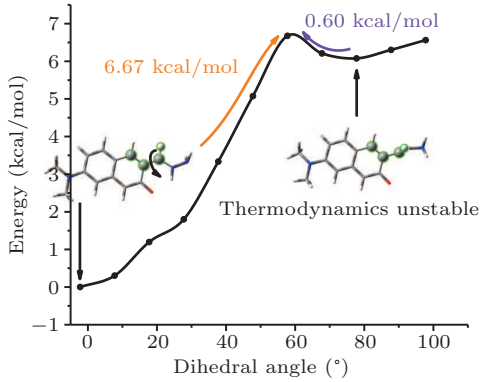


Fig. 8. The established potential energy curve for breaking intramolecular hydrogen bond structure in the S_1 state.

4. Conclusion

In conclusion, the detection for FA was implemented by condensation between the hydrazine moiety of Naph1 and the reactive carbon site of FA. Because of the importance of ESIPT reaction on fluorescent sensing mechanism, the ESIPT mechanism had been theoretically investigated with TDDFT methods and simulated by excited-state dynamics. The potential energy surface as a function of O–H bond length and dihedral angle CNNH was established, and the calculated reactive activation energy barrier of 0.51 kcal/mol indicated the spontaneous ESIPT coupled with dihedral torsion of the amino group about 77°. In order to in-depth illustrate the sensing mechanism, the potential energy curves between six lowest singlets and triplet excited states, and the non-adiabatic excited-state dynamics of three lowest singlet excited states were calculated and simulated, which indicated that the isomer of Naph1 had the deactivation process via the MECP of S_1/T_2 ISC. Based on the SA-CASSCF method in gas phase, the MECI of S_0/S_1 CI was nonexistent in the ESIPT process. Therefore, it concluded that the deactivation channel originated from S_1/T_2 ISC. Combined with FMOs analysis, the keto of product turned off the deactivation channel by the ESIPT without TICT, generating the strong fluorescent signal to realize the efficient detection for FA. Therefore, the theoretical dissection of the sensing mechanism was significant for the development of light-up ESIPT-based fluorescent probes to efficiently detect reactive carbon species.

Data availability statement

The data that support the findings of this study are openly available in Science Data Bank at

http://doi.org/10.57760/sciencedb.j00113.00038.

All relevant data supporting this study's findings are available from the corresponding authors upon reasonable request.

Acknowledgements

Project supported by the National Natural Science Foundation of China (Grant No. 12104392); the Natural Science Foundation of Hebei Province, China (Grant No. B2021203017); the High-Level Innovative Talents Program of Shenyang City (Grant No. RC200565); and the Innovation Capability Improvement Project of Hebei Province, China (Grant No. 22567605H). The numerical calculations in this paper have been done on the supercomputing system in the High-Performance Computing Center of Yanshan University.

References

[1] Ariyageadsakul P, Vchirawongkwin V and Kritayakornupong C 2016 *Sensor Actuat. B-Chem.* **232** 165
[2] Jass H E 1985 *History and Status of Formaldehyde in the Cosmetics Industry* (Advances in Chemistry of ACS Publications) pp. 229–236
[3] Meyer B and Hermanns K 1985 *Formaldehyde Release from Pressed Wood Products* (Advances in Chemistry of ACS Publications) pp. 101–116
[4] Scheuplein R J 1985 *Formaldehyde: The Food and Drug Administration's Perspective* (Advances in Chemistry of ACS Publications) pp. 237–245
[5] Organization W H, Formaldehyde, World Health Organization, 1989
[6] Tang X, Bai Y, Duong A, Smith M T, Li L and Zhang L 2009 *Environ. Int.* **35** 1210
[7] Tsukada Y I, Fang J, Erdjument-Bromage H, Warren M E, Borchers C H, Tempst P and Zhang Y 2006 *Nature* **439** 811
[8] Lu K, Craft S, Nakamura J, Moeller B C and Swenberg J A 2012 *Chem. Res. Toxicol.* **25** 664
[9] Merk O and Speit G 1998 *Environ. Mol. Mutagen.* **32** 260
[10] Zhao X Q and Zhang Z Q 2009 *Talanta* **80** 242
[11] Li F X, Lu J, Xu Y J, Tong Z Q, Me C L and He R Q 2008 *Prog. Biochem. Biophys.* **35** 393
[12] Kowatsch S *Formaldehyde in: Phenolic Resins: A Century of Progress*, Springer Inc, 2010, pp. 25–40
[13] Ohata J, Bruemmer K J and Chang C J 2019 *Accounts Chem. Res.* **52** 2841
[14] Liu X, Li N, Li M, Chen H, Zhang N, Wang Y and Zheng K 2020 *Coordin. Chem. Rev.* **404** 213109
[15] Chen W, Yang M, Luo N, Wang F, Yu R Q and Jiang J H 2019 *Analyst* **144** 6922
[16] He L, Yang X, Ren M, Kong X, Liu Y and Lin W 2016 *Chem. Comm.* **52** 9582
[17] Chang C J, James T D, New E J and Tang B Z 2020 *Accounts Chem. Res.* **53** 1
[18] Zhang H, Shao Z and Zhao K 2020 *Chin. Phys. B* **29** 083304
[19] Zhao J, Ji S, Chen Y, Guo H and Yang P 2012 *Phys. Chem. Chem. Phys.* **14** 8803
[20] Li G Y and Han K L 2018 *WIRES Comput. Mol. Sci.* **8** e1351
[21] Zheng J J, Lu Y Q, Li P L and Chen T 2010 *Acta Phys. Sin.* **59** 6626 (in Chinese)
[22] Song Y, Liu S, Lu J, Zhang H, Zhang C and Du J 2019 *Chin. Phys. B* **28** 093102
[23] Li Y Q, Ma Y Z, Yang Y F, Shi W, Lan R F and Guo Q 2018 *Phys. Chem. Chem. Phys.* **20** 4208
[24] Yang Y, Ding Y, Shi W, Ma F and Li Y 2020 *J. Lumin.* **218** 116836
[25] Zhao J and Jin B 2021 *J. Lumin.* **232** 117800
[26] Zhao J, Li Z and Jin B 2021 *J. Lumin.* **238** 118231
[27] Niu Y, Wang R, Shao P, Wang Y and Zhang Y 2018 *Chem. Eur. J.* **24** 16670
[28] Nagaoka S I, Endo H, Ohara K and Nagashima U 2015 *J. Phys. Chem. B* **119** 2525
[29] Tseng H W, Liu J Q, Chen Y A, Chao C M, Liu K M, Chen C L, Lin T C, Hung C H, Chou Y L, Wang T L and Chou P T 2015 *J. Phys. Chem. Lett.* **6** 1477
[30] Nagaoka S I, Nakamura A and Nagashima U 2002 *J. Photoch. Photobio. A* **154** 23
[31] Yang Y G, Liu Y F, Yang D P, Li H, Jiang K and Sun J F 2015 *Spectrochim. Acta A* **151** 814
[32] Sun C, Cao B, Yin H and Shi Y 2020 *Chin. Phys. B* **29** 058202
[33] Zhang X, Han J H, Li Y, Sun C F, Su X, Shi Y and Yin H 2020 *Chin. Phys. B* **29** 038201
[34] Seo J, Kim S and Park S Y 2004 *J Am. Chem. Soc.* **126** 11154
[35] Marenich A V, Cramer C J and Truhlar D G 2009 *J Phys. Chem. B* **113** 6378
[36] Cohen A J, Mori-Sánchez P and Yang W 2008 *Science* **321** 792
[37] Jacquemin D, Mennucci B and Adamo C 2011 *Phys. Chem. Chem. Phys.* **13** 16987
[38] Grimme S, Ehrlich S and Goerigk L 2011 *J. Comput. Chem.* **32** 1456
[39] Grimme S, Antony J, Ehrlich S and Krieg H 2010 *J. Chem. Phys.* **132** 154104
[40] Ruckenbauer M, Fazzi D, Arbelo-Gonzalez W and Barbatti M A 2016 *Tutorial for NEWTON-X* version 2.0
[41] Lu T http://sobereva.com/286 (Date of access: 27/03/2022).
[42] Harvey J, Aschi M, Schwarz H and Koch W 1998 *Theor. Chem. Acc.* **99** 95
[43] Miller W H, Handy N C and Adams J E 1980 *J. Chem. Phys.* **72** 99
[44] Frisch M J, Trucks G W, Schlegel H B, *et al.* 2013 *Gaussian 16* Revision A. 03 (Wallingford CT, Gaussian Inc.)
[45] Bruemmer K J, Walvoord R R, Brewer T F, Burgos-Barragan G, Wit N, Pontel L B, Patel K J and Chang C J 2017 *J. Am. Chem. Soc.* **139** 5338
[46] Schlegel H B 1982 *J. Comput. Chem.* **3** 214
[47] Yang Y F, Chen Y P, Zhao Y, Shi W, Ma F C and Li Y Q 2019 *J. Lumin.* **206** 326
[48] Zhao Y X, Wu X N, Ma J B, He S G and Ding X L 2010 *J. Phys. Chem. C* **114** 12271
[49] Zhao Y, Ding Y, Yang Y, Shi W and Li Y 2019 *Org. Chem. Front.* **6** 597
[50] Basarić N and Wan P 2006 *Photoch. Photobio. Sci.* **5** 656
[51] Zhao N, Li Y, Jia Y and Li P 2018 *J. Phys. Chem. C* **122** 26576
[52] Li C Z, Yang Y G, Ma C and Liu Y F 2016 *RSC Adv.* **6** 5134
[53] Zhao G J and Han K L 2007 *J. Phys. Chem. A* **111** 9218
[54] Li C Z, Yang Y G, Li D L and Liu Y F 2017 *Phys. Chem. Chem. Phys.* **19** 4802
[55] Zhao G J and Han K L 2007 *J. Phys. Chem. A* **111** 2469
[56] Li H, Han J, Zhao H, Liu X, Luo Y, Shi Y, Liu C, Jin M and Ding D 2019 *J. Phys. Chem. Lett.* **10** 748
[57] Andrienko G A Chemcraft 1.8 https://chemcraftprog.com/ (Date of access: 27/03/2022)
[58] Gutman I and Cyvin S J 1989 *Introduction to the Theory of Benzenoid Hydrocarbons* (Springer Inc.) pp. 51–77
[59] Nagaoka S, Hirota N, Sumitani M, Yoshihara K, Lipczynska-Kochany E and Iwamura H 1984 *J Am. Chem. Soc.* **106** 6913
[60] Nagaoka S, Hirota N, Sumitani M and Yoshihara K 1983 *J. Am. Chem. Soc.* **105** 4220